JOURNAL OF GEOPHYSICAL RESEARCH, VOL. 113, A04220, doi:10.1029/2007JA012681, 2008

Click Here for Full Article

Effect of solar wind variation on low-energy O^+ populations in the magnetosphere during geomagnetic storms: FAST observations

Y. Yao,[1] K. Seki,[1,2] Y. Miyoshi,[1] J. P. McFadden,[3] E. J. Lund,[4] and C. W. Carlson[3]

Received 24 July 2007; revised 21 November 2007; accepted 20 December 2007; published 23 April 2008.

[1] The relationship between solar wind conditions and variations in low-energy (<28 keV) O^+ ions during magnetic storms was investigated based on Fast Auroral Snapshot (FAST) observations. We selected four magnetic storms in 2000 using the following criteria: 1. the time profile of the *Dst* is simple (no multiple main phase), 2. the FAST orbit has a good coverage in the midnight and/or dusk side sector, and 3. middle-latitude (ILAT > 45°) particle data are available. For each orbit in the course of the four magnetic storms, the simultaneous solar wind data are compiled and the effects of each solar wind parameter such as the dynamic pressure, the dawn-dusk electric field, the velocity, and the density are investigated. The results indicate a strong correlation between the pressure and density of low-energy O^+ ions in the ring current region and the storm intensity, which is consistent with previous studies on high-energy (>50 keV) O^+ ions. The solar wind dynamic pressure also plays an important role in O^+ pressure and density enhancement in the ring current and plasma sheet regions.

Citation: Yao, Y., K. Seki, Y. Miyoshi, J. P. McFadden, E. J. Lund, and C. W. Carlson (2008), Effect of solar wind variation on low-energy O^+ populations in the magnetosphere during geomagnetic storms: FAST observations, *J. Geophys. Res.*, *113*, A04220, doi:10.1029/2007JA012681.

1. Introduction

[2] O^+ ions of ionospheric origin have been an interesting subject for a long time since the first definitive observation in the magnetosphere reported by *Shelley et al.* [1972]. These heavy O^+ ions have been studied by many previous studies [*Lennartsson*, 1991; *Yau and André*, 1997; *Daglis*, 1997; *Seki et al.*, 1998, 2002; *Moore et al.*, 1999; *Elliott et al.*, 2001; *Lennartsson et al.*, 2004; *Arvelius et al.*, 2005], but the role of these O^+ ions in the magnetospheric dynamics is far from clearly understood. The O^+ escaping from the ionosphere into the magnetosphere are known as ion outflows, which have been a hot topic studied by numerous polar orbiting satellites (Akebono, DE-1, Viking, Polar, FAST, etc.) (see *Yau and André* [1997] for a review). Recent studies, for instance Akebono/SMS observations [*Cully et al.*, 2003], indicated the dependence of lower-energy (≤70 eV) ion outflow on solar wind conditions. *Wilson et al.* [2004] investigated the ion outflow rates from the nightside auroral zone and polar cap as a function of the substorm phase using the Fast Auroral Snapshot/time-of-flight energy angle mass spectrograph (FAST/TEAMS) data. *Moore et al.* [2007] numerically studied the O^+ outflow from a viewpoint of the global circulation. Previous studies [*Young et al.*, 1982; *Lennartsson*, 1989] demonstrated the dependence of low-energy (≤16 keV) O^+ ion density in the near-earth and distant plasma sheet on solar F10.7 as a proxy of solar EUV.

[3] It is well known that the ring current plasma includes several ion species (H^+, O^+, He^+ and He^{++}), and we are interested in the contribution of O^+ ions to the ring current. Results from AMPTE and CRRES observations revealed that high-energy (>40 keV) O^+ ions mainly contribute the ring current during the main phase of large geomagnetic storms [*Daglis et al.*, 1999, and references therein]. *Nosé et al.* [2005] showed similar results from the Geotail data, and summarized the statistical results by showing that the O^+/H^+ energy density increases with the strength of the geomagnetic storms. On the other hand, observations of the AMPTE/CCE satellite showed that the contribution at low energies (≤30 keV) to the storm time ring current is small [*Gloeckler et al.*, 1985; *Stüdemann et al.*, 1986; *Hamilton et al.*, 1988].

[4] In this paper, we will investigate the low energy O^+ dynamics during storm times using the FAST observations. The terminology of "low energy" used in this study refers to the low energy part of the ring current ions up to 28 keV. The FAST satellite payload includes an instrument of a mass spectrograph, therefore it is possible to study ion composition and its energy density in the inner magnetosphere. We also investigate which solar wind parameter is

[1]Solar-Terrestrial Environment Laboratory, Nagoya University, Nagoya, Aichi, Japan.
[2]Also at Institute for Advanced Research, Nagoya University, Nagoya, Aichi, Japan.
[3]Space Sciences Laboratory, University of California, Berkeley, California, USA.
[4]Space Science Center, University of New Hampshire, Durham, New Hampshire, USA.

Copyright 2008 by the American Geophysical Union.
0148-0227/08/2007JA012681$09.00

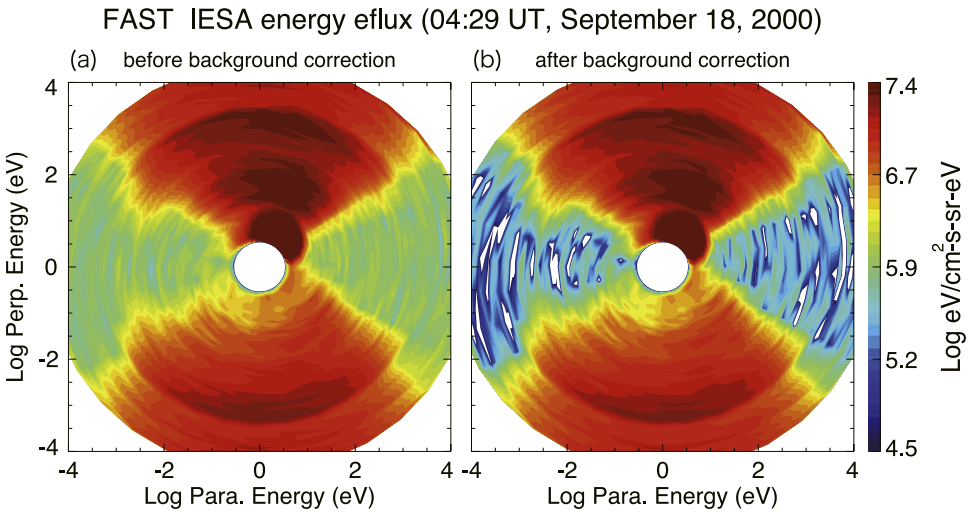

Figure 1. Distribution functions of IESA energy flux at 04:29 UT, 18 September 2000 (indicated by gray vertical line in Figure 2). The distribution functions (a) before background correction, and (b) after background correction are shown. Vertical and horizontal axes represent the perpendicular and parallel directions to the local magnetic field, respectively.

effective for the flux enhancement of O^+ ions in the ring current and plasma sheet regions.

2. Data Sets and Analysis Method

2.1. Data Sets

[5] We examine four magnetic storms in the year 2000, when it was the solar maximum of the 23rd solar cycle, based on the FAST satellite observations [*Pfaff et al.*, 2001]. The FAST satellite was launched on 21 August 1996 into a high-inclination (83°) elliptical orbit with apogee and perigee altitudes of 4175 km and 350 km, respectively. The orbital period was 133 min. In this study, we use the data obtained by Electrostatic Analyzer (ESA) [*Carlson et al.*, 2001] and the TEAMS [*Klumpar et al.*, 2001], a highly sensitive mass-resolving ion spectrometer. The ESA measures energy range from 4 eV to 30 keV for electrons and 3 eV to 28 keV for ions. The TEAMS was designed to measure the full 3-dimensional distribution function of major ion species (including H^+, He^+, He^{++} and O^+) in the lower-energy range up to 12 keV. The 3- and 2-dimensional distribution functions of each individual ion species can be determined with 2.5 s and 78 ms, respectively. The energy flux ratio of each ion species is provided from TEAMS as a function of energy. The energy flux of each ion species in the energy range above 12 keV to 28 keV was determined by extrapolation, and the energy flux ratio in this energy range was calculated with the extrapolated data. This ratio is multiplied by the ESA ion data to obtain 2-dimensional pitch angle distributions of O^+ and H^+ ions. There are two advantages in using the FAST observations. The first is the high temporal resolution. The second is that FAST can observe at middle latitudes.

[6] The particle data at middle latitudes are generally contaminated by the radiation belt electrons. In this study, we used an automated noise correction method, which subtracted the high-energy electron noise component from the original data using the count rate in the loss cone [*Seki et al.*, 2005]. The method consists of the following four steps. (1) We calculate average energy flux inside the loss cone in the upward direction for each energy bin. (2) Then the minimum of the average loss cone energy flux at a certain energy bin for each time step is saved. (3) After carrying out these procedures for a whole orbit, boxcar smoothing over time is conducted. (4) After conducting all steps both for electron and ion sensors, the smaller value of the two is used as a background noise and converted to count rate. Figure 1 is an example of the distribution functions of IESA energy flux before and after background correction. The distribution function was obtained at 04:29 UT, 18 September (indicated by gray vertical line in Figure 2) when the ESA background count rate reached the peak value. Comparing Figures 1a and 1b, a double loss cone structure can be seen in Figure 1b, while it is not clear in Figure 1a due to contamination.

[7] We selected the four storm events (11–15 February; 6–9 April; 24–26 May and 17–20 September) based on the following three selection criteria. (1) The *Dst* index has a simple structure in the storm main phase; (2) magnetic local time of the FAST satellite at about 60° invariant latitude (ILAT) must be within 17:00 and 01:30, i.e., from pre-dusk side to post-midnight and (3) before the storm there were no other intense storms of $Dst < -100$ nT within six days prior to storm commencement. For the storm period, we determined that the storm events must include the storm initial phase, the main phase and the recovery phase. In the recovery phase, the time when the *Dst* index recovers to −40 nT is defined as the end time of the storm.

[8] Figure 2 presents the FAST measurements from 04:20 to 05:08 UT on 18 September 2000. Both electrons and ions are in the low-energy range from 80 eV to 28 keV. Panels (a) and (b) illustrate the energy flux and pitch angle distribution of electrons, in which we can see intense electron precipitations in the auroral zone from 04:35 to 04:44 UT and from 04:56 to 05:03 UT. Around 04:30 UT, the energy flux of O^+ ions is more intense than that of H^+ ions in panels (c) and (d). On the other hand, H^+ ions have a stronger energy flux at much higher invariant latitudes.

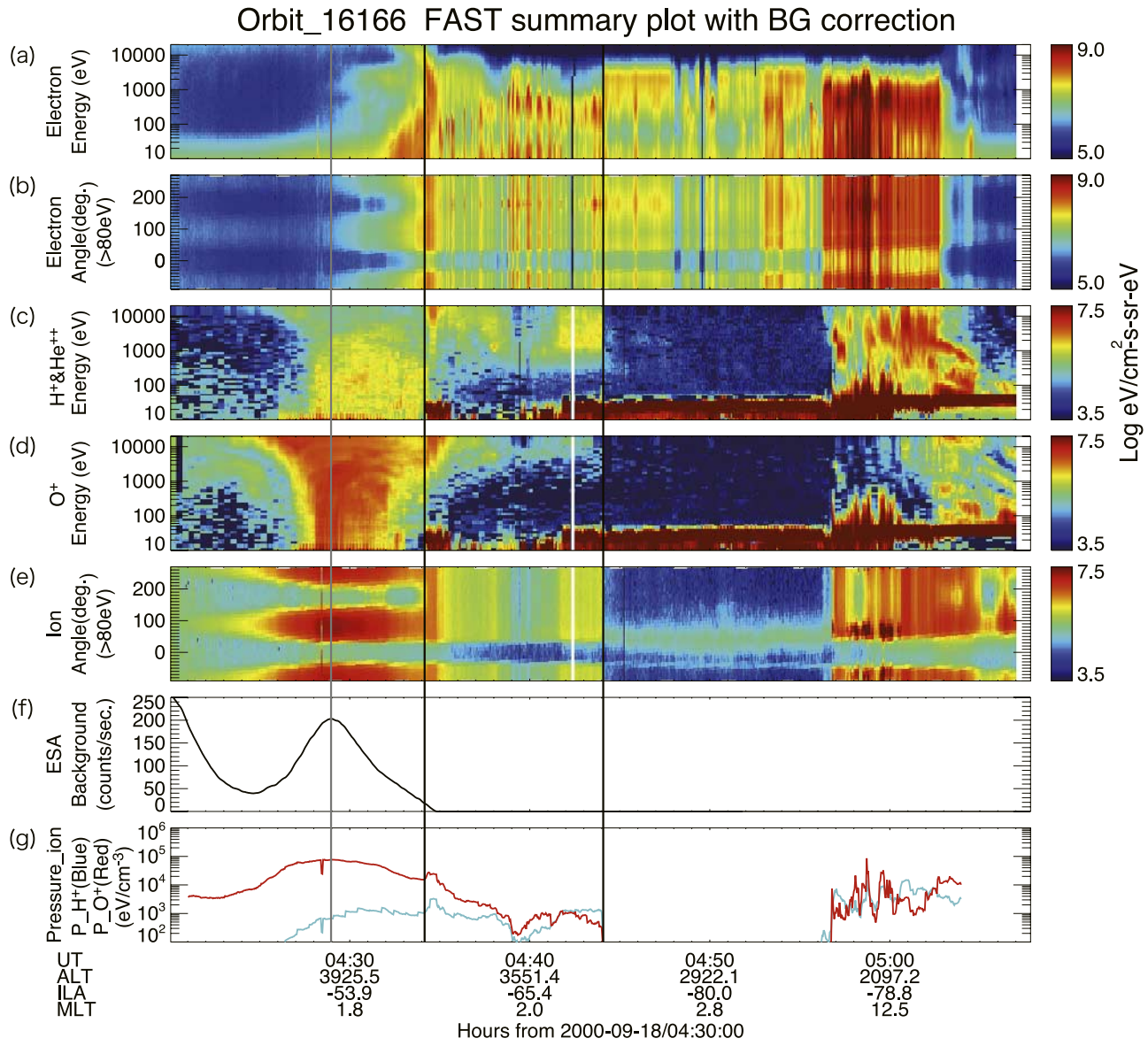

Figure 2. FAST one-orbit observations from 04:20 to 05:08 UT, 18 September 2000. (a, b) Energy flux and pitch angle distribution of electrons. (c) Energy flux of combinations of H^+ and He^{++} ions. (d) Energy flux of O^+ ions. (e) Pitch angle distribution of ions, which consist of four species: H^+, He^+, He^{++} and O^+. (f) Background counter of ESA. (g) Plasma pressure of ions: Blue and red lines refer to the pressure of H^+ and O^+, respectively.

From 05:03 UT to the end of the period, H^+ ions with one band structure and O^+ ions with multiple band structures are seen in both panels of (c) and (d). In panel (e), the plot of the ion pitch angle distribution shows double- and single-loss cone structures at different latitudes. Different loss cone distributions correspond to different magnetospheric regions. In this study, we identify the ring current region and plasma sheet region using the boundary between the double- and single-loss cones. Therefore from 04:20 to 04:34 UT, and from 04:34 to 04:44 UT, we define the ring current and plasma sheet regions, respectively. Panel (g) shows mean plasma pressure, and we can see high pressure in the ring current region. Near 04:59 UT, we can also find conics in panel (e), which should be one of the mechanisms of ion outflow. Panel (f) shows the background count of the ESA, which is a subtracted electron component with the automated noise correction. A peak in panel (f) should correspond to the outer belt, and the slot region at lower latitudes of the peak can also be seen.

2.2. Analysis Method

[9] Analysis method In this study, we try to estimate the contribution of low-energy O^+ ions to the *Dst* index. The current density perpendicular to the magnetic field at the equator in the ring current is a combination of the

magnetization current $\mathbf{J_M}$, the curvature drift current $\mathbf{J_R}$ and the grad-B drift current $\mathbf{J_B}$ [*Parker*, 1957], as follows:

$$\mathbf{J}_\perp = \mathbf{J_M} + \mathbf{J_R} + \mathbf{J_B} = \frac{\mathbf{B}}{B^2} \times \left[\nabla P_\perp + \left(P_\parallel - P_\perp\right) \frac{(\mathbf{B}\cdot\nabla)\mathbf{B}}{B^2} \right] \quad (1)$$

where $\mathbf{J}_\perp$, $P_\perp$ and $P_\parallel$ are the perpendicular current density, and the perpendicular and parallel components of the plasma pressure, respectively. $P_\perp$, and $P_\parallel$ are given by

$$P_\parallel = \int m v^2 f \cos^2\alpha \, dp \quad (2)$$

$$P_\perp = \int \frac{1}{2} m v^2 f \sin^2\alpha \, dp \quad (3)$$

where α and f are the pitch angle and the phase space density, respectively. FAST is a low-altitude polar orbit satellite, which can observe only particles with small pitch angle at the equator. Moreover, it is not possible to estimate magnetic local time distribution of particles from a single point observation. Therefore in the present work, we made two assumptions to derive the ring current: (1) $P_\perp = P_\parallel$ at the equator; (2) the ring current displays geometric symmetry during the geomagnetic storms. As a result, in equation (1), the second term of the right-hand side then disappears, and we can rewrite it as

$$\mathbf{J}_\perp = \frac{\mathbf{B}}{B^2} \times \nabla P_\perp. \quad (4)$$

That is, the perpendicular current density only depends on the magnetic field and the perpendicular pressure gradient. After calculating the $\nabla P_\perp$ term in equation (4) for obtaining the perpendicular current density, the magnetic disturbance induced by the current can be derived from the Biot-Savart law. The magnetic disturbance parallel to the Earth's dipole magnetic field at the center of the Earth, B_C, is given by

$$B_C = \frac{\mu_0}{4\pi} \int_r \int_\lambda \int_\phi \cos^2\lambda J_\phi(r,\lambda,\phi) dr d\lambda d\phi \quad (5)$$

where J_ϕ is the azimuthal component of $J_\perp$, which is given as follows:

$$J_\phi = \frac{1}{B^2}\left(\frac{B_r}{r}\frac{\partial P_\perp}{\partial \lambda} - B_\lambda \frac{\partial P_\perp}{\partial r}\right) + \frac{1}{B^3}\left(P_\parallel - P_\perp\right) \cdot \left(\frac{B_r}{r}\frac{\partial B}{\partial \lambda} - B_\lambda \frac{\partial B}{\partial r}\right).$$

From these two assumptions, we can further rewrite equation (6) as

$$J_\phi(r) = \frac{B}{B^2}\frac{\partial P}{\partial r} \quad (7)$$

and equation (5) as

$$B_C = \mu_0 \int_r J_\phi(r)\, dr. \quad (8)$$

[10] Here, we mention the limits of this estimation. Since the pitch angle distribution of the ring current ions is not purely isotropic but has significant anisotropy, the first assumption induces an underestimation of the current because the second term of the right-hand side of equation (1) does not contribute. The second assumption causes an overestimation of the current, because we used the data obtained within 17:00–01:30 MLT and the actual ring current shows strong enhancement in dusk and midnight sectors, especially during the main phase [*Maurice et al.*, 1998; *Ebihara and Ejiri*, 2000; *Jorgensen et al.*, 2004; *Jordanova and Miyoshi*, 2005]. Thus the estimated current has several ambiguities of amplitude, therefore, we will qualitatively discuss the time-spatial evolution of the ring current in this paper.

3. Observations

[11] Figures 3–6 show the outlines of these four geomagnetic storms. The first three panels represent the interplanetary electric field y component, the dynamic pressure of the solar wind measured by the Advanced Composition Explorer (ACE) and the *AU*, *AL* indices, respectively. The fourth panel shows the *Dst* index (black) and the corrected *Dst* index (green) using the solar wind dynamic pressure [e.g., *Ebihara and Ejiri*, 2000]; the red and blue dotted lines refer to the contributions from the estimated ring current of O^+ and H^+ ions from the method described in section 2.2. *L*-time diagrams of H^+ and O^+ ion plasma pressure and perpendicular current density distribution are shown in panels (g) and (h), and the integral mean pressure and density of H^+ and O^+ ions are shown in the last two panels. Each vertical column of the *L*-time diagrams corresponds to one orbit of the FAST satellite.

3.1. 12 February 2000 Storm

[12] Figure 3 shows the February 2000 storm. The main phase started at 08:00 UT, 12 February 2000, continued for about three hours. The *Dst* index showed its minimum value as −133 nT. In the second panel, we can see that an interplanetary shock arrived near 23:30 UT, 11 February 2000, and the other pressure jump came with a strong fluctuation of the solar wind dynamic pressure. The solar wind dynamic pressure decreased after the second pressure jump. The IMF B_z turned southward (positive electric field) during the first shock arrival. After remaining southward for about 1 hour, the IMF B_z turned northward again. At this time a strong substorm occurred as shown in the *AL* index. A second large substorm occurred during the storm main phase, which may have worked as a driver for particle injection to the ring current region. In the bottom panel, the mean density of H^+ and O^+ ions in different regions kept increasing from 05:00 UT, 12 February after the first substorm. At 07:30 UT, 12 February, the IMF B_z turned southward again, and continued for about three hours. The storm occurred simultaneously with this southward turning. We can find that the pressure of O^+ ions was very high in the *L* range from 2 to 5. As compared to the O^+ ions, the pressure of H^+ ions was low in the low *L* region (panel f), but was relatively high in the high *L* region. It is revealed that low-energy H^+ ions did not significantly contribute to the ring current. The percentage of the contribution from the

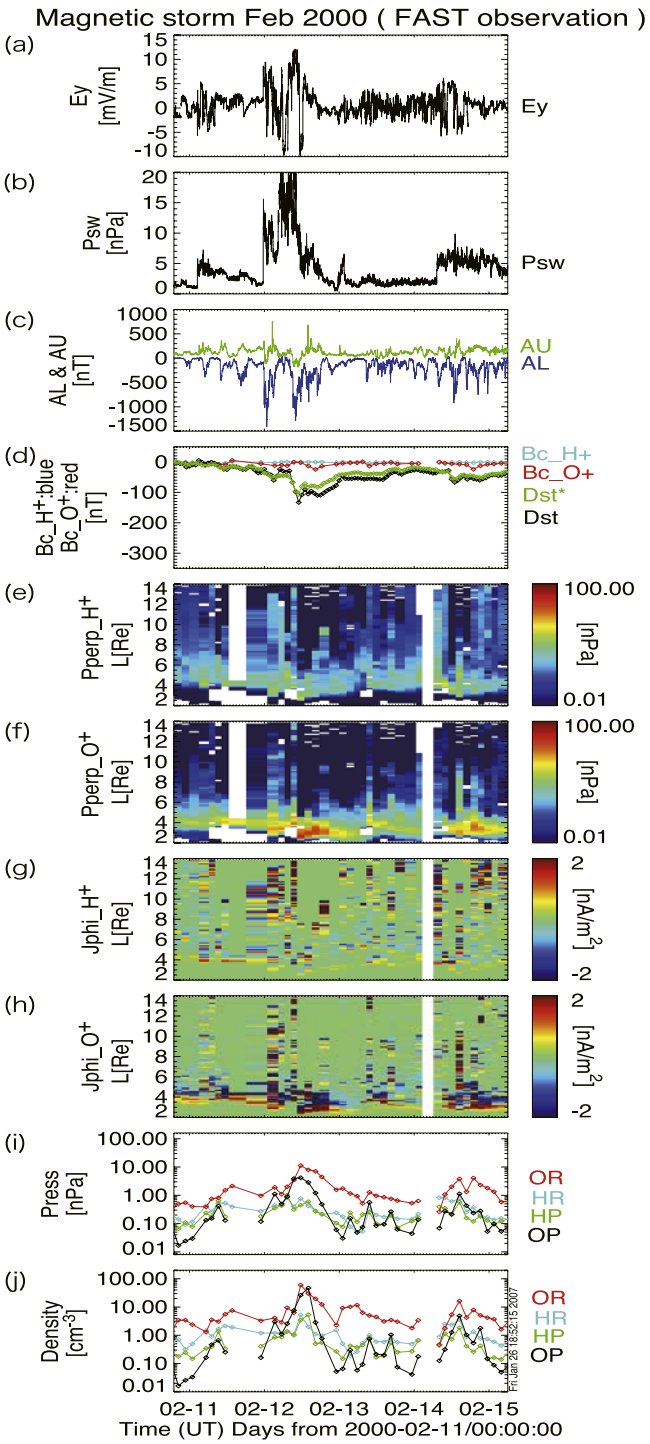

Figure 3. Outline of the 12 February geomagnetic storm. Panels (a) and (b) refer to interplanetary electric field and solar wind dynamic pressure, respectively. Panels (c) and (d) show the AU, *AL* and *Dst* indices. In panels (e)-(h), the distribution of plasma pressure (H^+ and O^+ ions) and current density (H^+ and O^+ ions) are shown. (i) and (j) represent the mean plasma pressure and density of H^+ and O^+ ions in different regions. Marks OR, HR, HP and OP on the right hand of panels (i) and (j) refer to the O^+ (O) and H^+ (H) ions in the ring current (R) and plasma sheet (P) regions.

O^+ ions to the ring current on the *Dst* index reaches to about 10 percent, while that of the H^+ ions is negligible. In the seventh and eighth panels, the equatorial current density for the H^+ ions shows no westward currents in the ring current region, while we can clearly see the westward currents for the O^+ ions in the same region. We also see that there was an eastward ring current within 3 R_E consisting only of O^+ ions. Such eastward ring current is natural, considering that the ring current is driven by the pressure gradient as shown

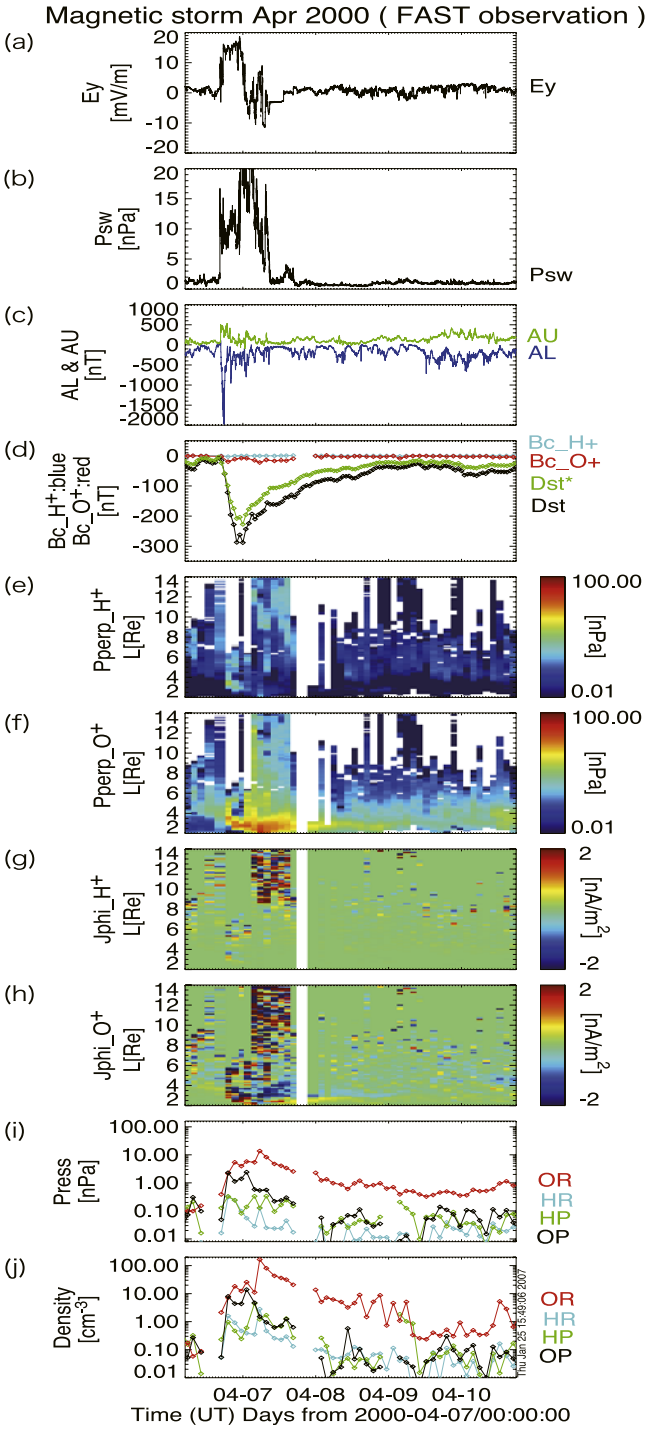

Figure 4. Outline of the 7 April geomagnetic storm. The panel format is the same as that of Figure 3.

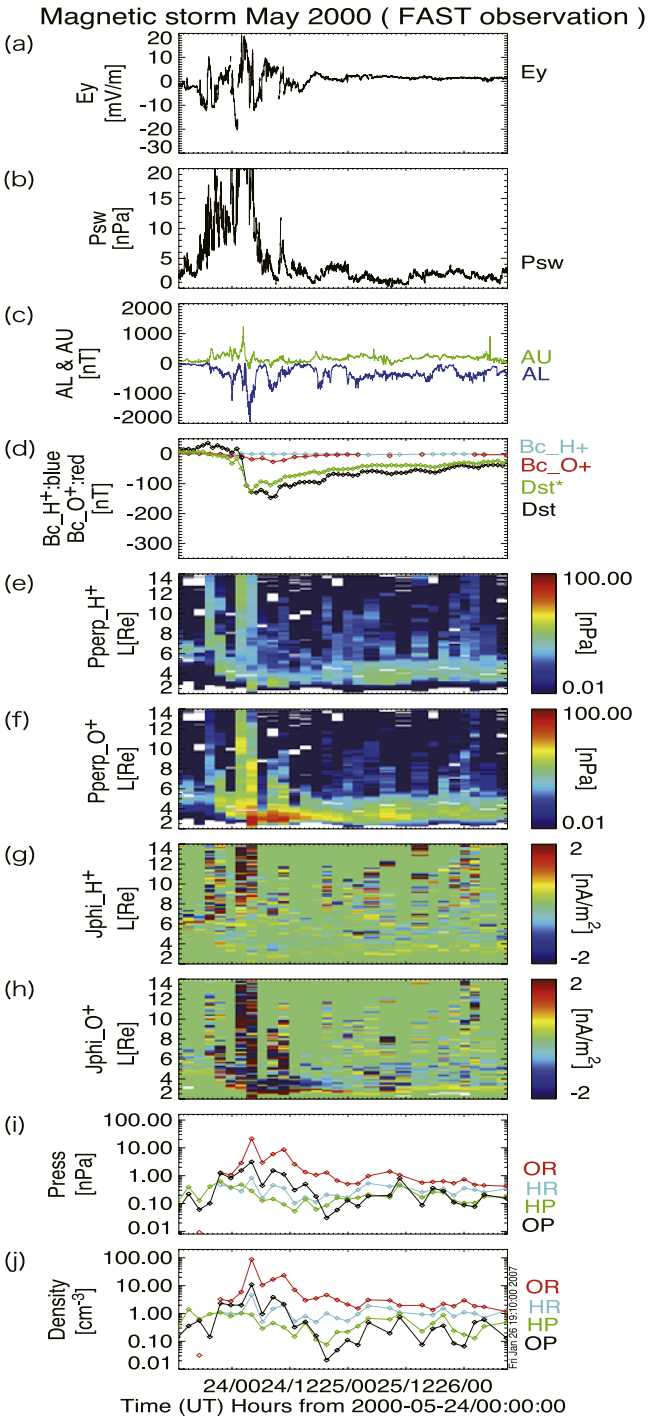

Figure 5. Outline of the 24 May geomagnetic storm. The panel format is the same as that of Figure 3.

in equation (4), and this current distribution driven by low-energy O^+ ions is consistent with other studies showing the total ring current structure [e.g., *Lui et al.*, 1987; *Le et al.*, 2004].

3.2. 6 April 2000 Storm

[13] The April 2000 storm is shown in Figure 4. The minimum *Dst* index of this storm was −288 nT. The storm began simultaneously with the shock arrival at 16:00 UT, 6 April. At this time, a strong substorm occurred. During the main phase, the second interplanetary shock arrived. A very strong substorm, $AE \sim 2000$ nT, occurred associated with the shock. Moreover, during the main phase, the pressure distribution of O^+ ions also started to change. The pressure of the O^+ ions increased from $L = 2$ to 6 during the main phase. We can see that the peak position of the O^+ ions pressure was moving inward near about 3 R_E. In the storm

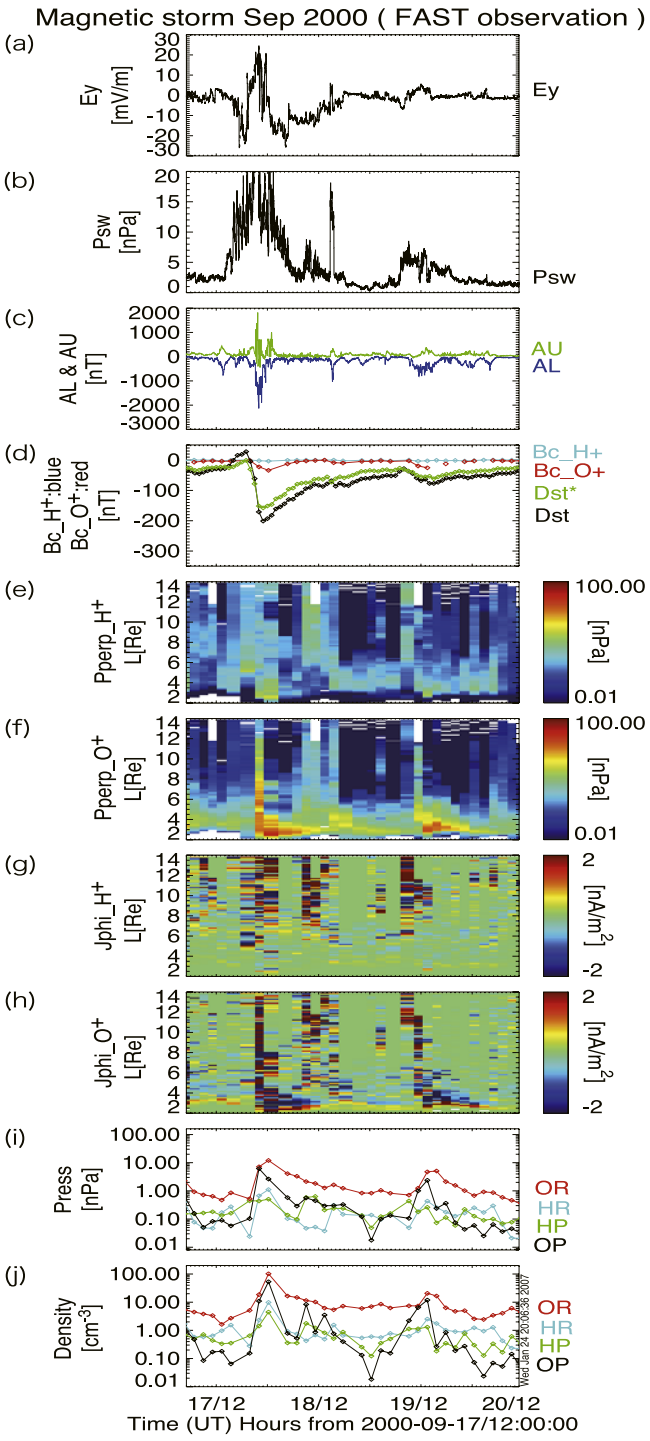

Figure 6. Outline of the 18 September geomagnetic storm. The panel format is the same as that of Figure 3.

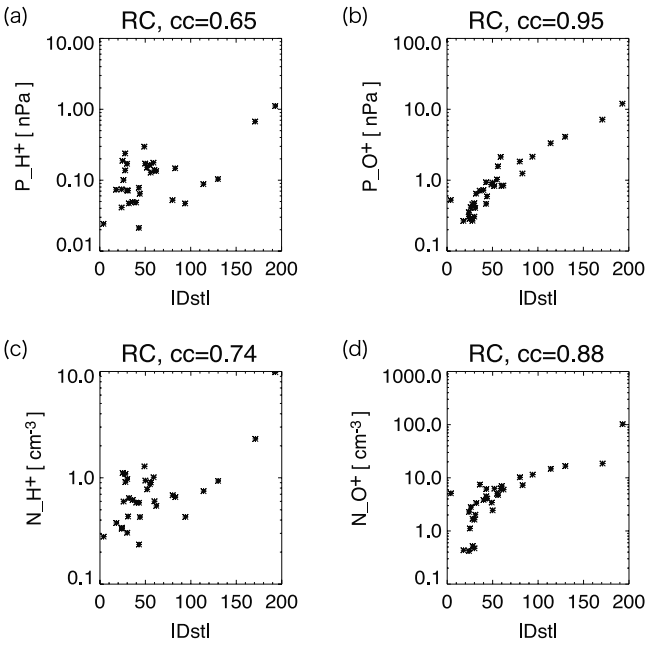

Figure 7. Relationship between storm intensity and pressure (top) and density (bottom) of ions in the ring current region. The two left-hand plots refer to the H^+ ions, and the right-hand plots refer to the O^+ ions. The correlation coefficient is shown in each panel.

early recovery phase, around 04:00 UT, 7 April, the high-pressure region of the O^+ ions expanded to higher *L*-region. Compared to the O^+ ions, the pressure distribution of H^+ ions did not show a violent variation during the storm period. In this event, the contribution from the O^+ ions reaches about 5 percent, while the contribution from the H^+ ions is negligible.

3.3. 24 May 2000 Storm

[14] Figure 5 shows the May 2000 storm. The storm size of this event is not very large; the *Dst* index reaches its minimum value of −147 nT. Solar wind dynamic pressure had increased about eight hours before the storm commencement. At about 00:30 UT, 24 May, which was the commencement of the storm, solar wind pressure increased sharply to a higher value. In the storm main phase and early recovery phase, there were two substorms with different levels. The first one was very strong, which may have been related to the pressure jump of the solar wind. The second one was relatively small; the maximum *AE* value was about 1000 nT. In this storm, the pressure distribution of the H^+ ions shows a similar variation compared to the O^+ ions. The pressure of the O^+ ions started to increase before the storm main phase relative to the increase of the solar wind pressure. In this storm, we can also find the peak pressure value of O^+ ions located at L ∼ 3. In the main phase, about 03:00 UT, 24 May, the pressure distribution of the O^+ ions showed an expanded structure, which extended to a distant place in the plasma sheet. The perpendicular current density of the O^+ ions also shows a westward current that contributes to the storm-time ring current. The contribution from the O^+ ions attains about 10 percent, while that from the H^+ ions is negligible.

3.4. 18 September 2000

[15] Figure 6 is the September 2000 storm with the minimum *Dst* value as −201 nT. During this storm event, we can find some similar features to the May 2000 storm. Solar wind pressure started to simultaneously increase with the IMF B_z turning southward before the storm time. The IMF B_z began to turn southward at 19:00 UT, 17 September, and continued for about four hours. In the storm main phase, solar wind pressure started to decrease accompanied by very strong fluctuation; this fluctuation is a characteristic of this storm. In the slow recovery phase, there are other small substorms related to a pulse of solar wind pressure at 15:00 UT, 18 September. We can find that the pressure distribution of the O^+ ions began to increase sharply at about 20:00 UT, 17 September. Then, the pressure of the O^+ ions increased to a very high level and extended to a higher *L*-shell. It is found that the westward current of the O^+ ions flows in the near Earth region from $L = 2$ to 6, and the westward current of the H^+ ions flows in a distant range over $L = 6$. The minimum value of the *Dst* index in this event exceeded −200 nT. The mean contribution percentage of the ring current from the O^+ ions is about 10 percent, while the contribution from the H^+ ions is negligible.

3.5. Comparison With Solar Wind Parameters

[16] Figure 7 shows the average pressure or density of the O^+ ions and the H^+ ions during each FAST orbit as a function of the amplitude of the *Dst* index for the September 2000 storm. As same as previous studies for high-energy O^+ ions [e.g., *Daglis*, 1997], the energy density of the low-energy O^+ ions increases as the *Dst* index decreases, and reaches its peak as *Dst* decreases to its minimum. The correlation coefficients in the ring current region between the *Dst* index and the pressure and density of the O^+ ions are 0.95 and 0.88, respectively. In the plasma sheet region, the correlation coefficients of O^+ ions are 0.82 and 0.74. These results indicate that O^+ ions increase substantially both in the ring current and plasma sheet regions during the intense storm. The correlation coefficients of the H^+ ion pressure and density with the *Dst* index are smaller, 0.65 and 0.74 in the ring current region, and 0.34 and 0.51 in the plasma sheet region respectively.

[17] We calculated the correlation with solar wind pressure (P_{sw}) and the standard deviation of solar wind pressure (σ_{Psw}). The 64-second averaged IMF and solar wind ion data of the ACE satellite have been used for the calculation. The solar wind data is averaged for the period when the FAST satellite traversed plasma sheet and ring current regions. In Figure 8, the correlation coefficients between the σ_{Psw} and the O^+ ion pressure and density are shown in both the ring current and plasma sheet regions. In the ring current region, the coefficients between σ_{Psw} and the pressure and density of the O^+ ions are 0.62 and 0.61, respectively. In the plasma sheet region, their coefficients are 0.76 and 0.74, respectively. It is also found that the pressure and density of the ring current O^+ ions show relatively good correlations with σ_{Psw} compared to the solar wind dynamic pressure itself. As for the H^+ ion, the results show that the P_{sw} and σ_{Psw} do not correlate with the H^+ ion

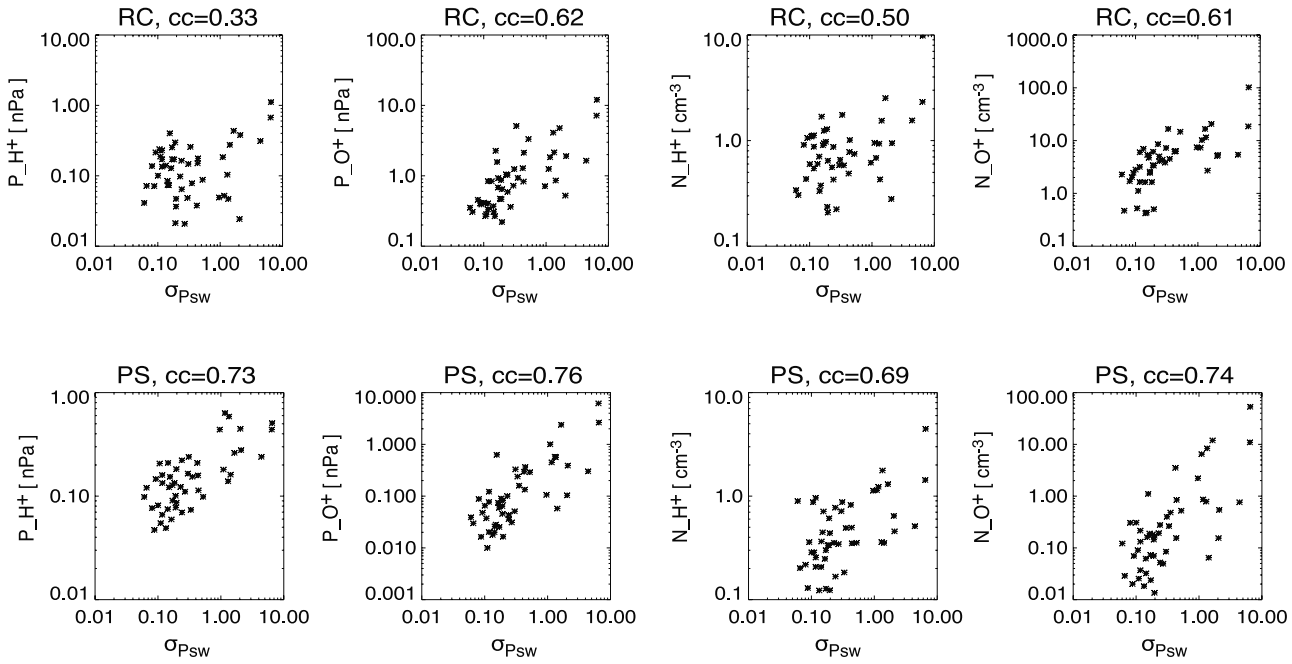

Figure 8. Scatter diagram for the standard deviation of solar wind pressure and pressure (left two columns) and density (right two columns) of H^+ and O^+ ions in the ring current region (top), and the plasma sheet region (bottom). The correlation coefficient is shown in each panel.

pressure and density in the ring current region. On the other hand, H^+ ion pressure and density in the plasma sheet region show good correlation both with the P_{sw} and σ_{Psw}.

[18] As shown in panel (i) of the Figures 3 to 6, the O^+ pressure in the ring current and plasma sheet regions show a different trend. The O^+ pressure in both regions started to increase at roughly the same time accompanied by the jump of the solar wind dynamic pressure. Then the O^+ pressure in the ring current region decreased slowly compared to that in the plasma sheet. That is, the pressure of the plasma sheet responses more directly to the solar wind disturbance than that of the ring current. The difference may be caused by the different loss mechanisms of O^+ in each region.

4. Discussion

[19] Using the TEAMS onboard the FAST satellite and ACE data, we investigated the contribution from low-energy (<28 keV) ions to the storm-time ring current, and the solar wind conditions for the ions variation. The results indicate that the pressure and density of O^+ ions have a good correlation with the *Dst* index and σ_{Psw} in both ring current and plasma sheet regions during the intense geomagnetic storms.

4.1. *Dst* Index and Low-Energy O^+ Ions

[20] Previous results demonstrated that high-energy O^+ ions carry a significant amount of the energy density of the outer ring current (L = 5–7) during the magnetic storms, and that the O^+/H^+ energy density ratio increased during storm time compared to quiet time [*Daglis*, 1997]. In this study, we found that the logarithm of the pressure and density of the O^+ ions and the *Dst* index have a good correlation. This indicates that the pressure and density of the O^+ ions at the low energy part and the *Dst* index have a nonlinear relation with each other. *Fu et al.* [2001] demonstrated statistical results of high-energy O^+ ions based on CRRES observations. The results show that the relationship between O^+ ion energy density and the *Dst* index is not linear, but it can be fit as an exponential function. AMPTE and CRRES data were used to statistically estimate the contribution of the main ion species to the total ion energy density at L = 5 [*Daglis et al.*, 1999]. The contribution from ionospheric O^+ ions is more than 60 percent during intense storms within the energy range from 1 to 430 keV. The low-energy part of the O^+ ions studied in this paper seems to be similar to the high-energy part, i.e., O^+ ion pressure and density increase during the storm main phase. However, the contribution from the low-energy part of the O^+ ions is limited. During the four intense storms examined in this study, the maximum contribution was no more than about 15 percent, although the estimation should have some ambiguities. This result is consistent with the previous studies [*Gloeckler et al.*, 1985; *Stüdemann et al.*, 1986; *Hamilton et al.*, 1988].

4.2. Solar Wind Dynamic Pressure and Low-Energy O^+ Ions

[21] In the previous studies, the following two processes have been considered as mechanisms for changing the ion population in the magnetosphere. One is that solar wind conditions control the variation of the plasma sheet properties [*Borovsky et al.*, 1998; *Thomsen et al.*, 1998; *Yan et al.*, 2005], and another is that solar wind conditions control the ionospheric ion outflow [*Moore et al.*, 1999; *Elliott et al.*, 2001; *Cully et al.*, 2003]. *Borovsky et al.* [1998] statistically studied the coupling of the plasma sheet to the solar wind using the ISEE-2 data. The results revealed that the particle pressure and the total pressure of the plasma sheet are

strongly correlated with the ram pressure of the solar wind, with coefficients of 0.84 and 0.85, respectively. Recently, Double Star (TC-1) observations [*Yan et al.*, 2005] also reported the same results, showing that the solar wind dynamic pressure significantly controls the ion thermal pressure in the near-earth plasma sheet. Note that their studies did not consider the ion species. *Nosé et al.* [2003] considered from a case study that variation of the ionospheric ions in the plasma sheet can be attributed to the solar wind dynamic pressure. Our results concerning the correlation between O^+ ion pressure and solar wind dynamic pressure are consistent with *Nosé et al.* [2003], but the energy range of our study is different from theirs.

[22] Our studies revealed that the standard deviation of the solar wind dynamic pressure correlated with the low-energy O^+ ions in the ring current region. Since the CRRES observation concerning the O^+ ions was for the high-energy part and did not study the correlation with solar wind conditions, the results of this study are new findings. The good correlation between O^+ ions and the standard deviation of the solar wind dynamic pressure is also found in the plasma sheet.

[23] The origin of the O^+ ions in the plasma sheet and the ring current is upwelling O^+ ions in the ionosphere. In fact, *Peroomian et al.* [2006] found using global MHD and test particle simulation that the dayside ion fountain supplies a significant amount of tens of keV O^+ ions to the plasma sheet and ring current during storm times. *Moore et al.* [1999] investigated the variation in ionospheric upwelling O^+ ions in response to a CME, and they suggested that these are controlled by the solar wind dynamic pressure disturbance. Since the four storms in this study were driven by CMEs, it is possible to consider that upwelling O^+ ions increased due to the fluctuation of solar wind dynamic pressure during the storms. Therefore good correlation between the O^+ ions in the plasma sheet and the ring current and the standard deviation of solar wind dynamic pressure in this study maybe due to the enhancement of upwelling ionospheric ions. The observations are consistent with the increase of polar O^+ outflows with increasing geomagnetic activities [e.g., *Yau et al.*, 1988].

[24] It should be noted that the ion transportation process from the ionosphere to the plasma sheet and ring current is also important. Mechanisms for the transportation and acceleration of upwelling O^+ ions have not been confirmed, and there may be a possibility that solar wind dynamic pressure fluctuations affect the mechanisms for the transportation and acceleration processes. This point will be a subject of our future study.

5. Summary

[25] In this study, we have investigated the variation of low-energy (<28 keV) O^+ ions in the inner magnetosphere using the FAST observations and examined the relationship with the solar wind conditions. We have subtracted the effect of high-energy radiation belt electrons and successfully derived the flux of several kinds of ions below 28 keV in the inner magnetosphere. We found a strong correlation between the pressure and density of low-energy O^+ ions in the ring current region and the storm intensity. This is consistent with previous work on high-energy (>50 keV) O^+ ions. Moreover, we newly found that the fluctuation of solar wind dynamic pressure is an important factor for the increase of the density and pressure of O^+ ions in both the ring current and plasma sheet regions.

[26] **Acknowledgments.** This work was supported by the 21st Century COE Program of Nagoya University ("Dynamics of the Sun-Earth-Life Interactive System"), Ryugaku Ikuei Scholarship of Daiko Foundation, and grant-in-aid for scientific research (18740309) from Ministry of Education, Culture, Sports, Science and Technology, Japan. JPM, EJL, and CWC were supported by NASA grant NAG5-12590. The author would also like to thank the world Data Center C2 at Kyoto, Japan for the geomagnetic indices: *Dst*, *AL* and *AU*, and the ACE spacecraft team for the ACE solar wind and magnetic field data.

[27] Wolfgang Baumjohann thanks the reviewers for their assistance in evaluating this paper.

References

Arvelius, S., et al. (2005), Statistics of high-altitude and high-latitude O^+ ion outflows observed by Cluster/CIS, *Ann. Geophys.*, *23*, 1909–1916.

Borovsky, J. E., M. F. Thomsen, and R. C. Elphic (1998), The driving of the plasma sheet by the solar wind, *J. Geophys. Res.*, *103*, 17,617–17,639.

Carlson, C. W., J. P. McFadden, P. Turin, and D. W. Curtis (2001), The electron and ion plasma experiment for FAST, *Space Sci. Rev.*, *98*, 33–66.

Cully, C. M., E. F. Donovan, A. W. Yau, and G. G. Arkos (2003), Akebono/suprathermal mass spectrometer observations of low-energy ion outflow: Dependence on magnetic activity and solar wind conditions, *J. Geophys. Res.*, *108*(A2), 1093, doi:10.1029/2001JA009200.

Daglis, I. A. (1997), The role of magnetosphere-ionosphere coupling in magnetic storm dynamics, in *Magnetic Storms, Geophys. Monogr. Ser.*, vol. 98, edited by B. T. Tsurutani et al., pp. 107–116, AGU, Washington, D. C.

Daglis, I. A., R. M. Thorne, W. Baumjohann, and S. Orsini (1999), The terrestrial ring current: Origin, formation, and decay, *Rev. Geophys.*, *37*, 407–438.

Ebihara, Y., and M. Ejiri (2000), Simulation study on fundamental properties of the storm-time ring current, *J. Geophys. Res.*, *105*(A7), 15,843–15,859.

Elliott, H. A., R. H. Comfort, P. D. Craven, M. O. Chandler, and T. E. Moore (2001), Solar wind influence on the oxygen content of ion outflow in the high-altitude polar cap during solar minimum conditions, *J. Geophys. Res.*, *106*(A4), 6067–6084.

Fu, S. Y., Q.-G. Zong, B. Wilken, and Z. Y. Pu (2001), Temporal and spatial variation of the ion composition in the ring current, *Space Sci. Rev.*, *95*, 539–554.

Gloeckler, G., B. Wilken, W. Stüdemann, F. M. Ipavich, D. Hovestadt, D. C. Hamilton, and G. Kremser (1985), First composition measurement of the bulk of the storm-time ring current (1 to 300 keV/e) with AMPTE-CCE, *Geophys. Res. Lett.*, *12*(5), 325–328.

Hamilton, D. C., G. Gloeckler, F. M. Ipavich, W. Stüdemann, B. Wilken, and G. Kremser (1988), Ring current development during the great geomagnetic storm of February 1986, *J. Geophys. Res.*, *93*(A12), 14,343–14,355.

Jordanova, V. K., and Y. Miyoshi (2005), Relativistic model of ring current and radiation belt ions and electrons: Initial results, *Geophys. Res. Lett.*, *32*, L14104, doi:10.1029/2005GL023020.

Jorgensen, A. M., H. E. Spence, W. J. Hughes, and H. J. Singer (2004), A statistical study of the global structure of the ring current, *J. Geophys. Res.*, *109*, A12204, doi:10.1029/2003JA010090.

Klumpar, D. M., et al. (2001), The time-of-flight energy, angle, mass spectrograph (TEAMS) experiment for FAST, *Space Sci. Rev.*, *98*, 197–219.

Le, G., C. T. Russell, and K. Takahashi (2004), Morphology of the ring current derived from magnetic field observations, *Ann. Geophys.*, *22*, 1267–1295.

Lennartsson, W. (1989), Energetic (0.1- to 16-keV/e) magnetospheric ion composition at different levels of solar F10.7, *J. Geophys. Res.*, *94*(A4), 3600–3610.

Lennartsson, W. (1991), Solar control of the Earth's emission of energetic O^+, *J. Atmos. Terr. Phys.*, *53*, 1103–1111.

Lennartsson, O. W., H. L. Collin, and W. K. Peterson (2004), Solar wind control of Earth's H^+ and O^+ outflow rates in the 15-eV to 33-keV energy range, *J. Geophys. Res.*, *109*, A12212, doi:10.1029/2004JA010690.

Lui, A. T. Y., R. W. McEntire, and S. M. Krimigis (1987), Evolution of the ring current during two geomagnetic storms, *J. Geophys. Res.*, *92*(A7), 7459–7470.

Maurice, S., M. F. Thomsen, D. J. McComas, and R. C. Elphic (1998), Quiet time densities of hot ions at geosynchronous orbit, *J. Geophys. Res.*, *103*(A8), 17,571–17,585.

Moore, T. E., W. K. Peterson, C. T. Russell, M. O. Chandler, M. R. Collier, H. L. Collin, P. D. Craven, R. Fitzenreiter, B. L. Giles, and C. J. Pollock

(1999), Ionospheric mass ejection in response to a CME, *Geophys. Res. Lett.*, *26*(15), 2339–2342.

Moore, T. E., M.-C. Fok, D. C. Delcourt, S. P. Slinker, and J. A. Fedder (2007), Global aspects of solar wind-ionosphere interactions, *J. Atmos. Sol. Terr. Phys.*, *69*, 265–278.

Nosé, M., R. W. McEntire, and S. P. Christon (2003), Change of the plasma sheet ion composition during magnetic storm development observed by the Geotail spacecraft, *J. Geophys. Res.*, *108*(A5), 1201, doi:10.1029/2002JA009660.

Nosé, M., S. Taguchi, K. Hosokawa, S. P. Christon, R. W. McEntire, T. E. Moore, and M. R. Collier (2005), Overwhelming O^+ contribution to the plasma sheet energy density during the October 2003 superstorm: Geotail/EPIC and IMAGE/LENA observations, *J. Geophys. Res.*, *110*, A09S24, doi:10.1029/2004JA010930.

Parker, E. N. (1957), Newtonian development of the dynamical properties of ionized gases of low density, *Phys. Rev.*, *107*, 924–933.

Peroomian, V., M. El-Alaoui, M. A. Abdalla, and L. M. Zelenyi (2006), Dynamics of ionospheric O^+ ions in the magnetosphere during the 24–25 September 1998 magnetic storm, *J. Geophys. Res.*, *111*, A12203, doi:10.1029/2006JA011790.

Pfaff, R., C. W. Carlson, J. Watzin, D. Everett, and T. Gruner (2001), An overview of the Fast Auroral Sanpshot (FAST) satellite, *Space Sci. Rev.*, *98*, 1–32.

Seki, K., M. Hirahara, T. Terasawa, T. Mukai, Y. Saito, S. Machida, T. Yamamoto, and S. Kokubun (1998), Statistical properties and possible supply mechanisms of tailward cold O^+ beams in the lobe/mantle regions, *J. Geophys. Res.*, *103*(14), 4477–4490.

Seki, K., R. C. Elphic, M. F. Thomsen, J. Bonnell, J. P. McFadden, E. J. Lund, M. Hirahara, T. Terasawa, and T. Mukai (2002), A new perspective on plasma supply mechanisms to the magnetotail from a statistical comparison of dayside mirroring O^+ at low altitudes with lobe/mantle beams, *J. Geophys. Res.*, *107*(A4), 1047, doi:10.1029/2001JA900122.

Seki, K., J. P. McFadden, R. C. Elphic, M. F. Thomsen, G. D. Reeves, Y. Yao, E. J. Lund, J. W. Bonnell, and C. W. Carlson (2005), On variation of outer radiation belt electrons and O^+ ions in the inner magnetosphere during large magnetic storms: FAST observations, *AGU, Fall Meet.*, Abstract SA12A-01.

Shelley, E. G., R. G. Johnson, and R. D. Sharp (1972), Satellite observations of energetic heavy ions during a geomagnetic storm, *J. Geophys. Res.*, *77*(31), 6104–6110.

Stüdemann, W., G. Gloeckler, B. Wilken, F. M. Ipavich, G. Kremser, D. C. Hamilton, and D. Hovestadt (1986), Ion composition of the bulk ring current during a magnetic storm: Observations with the CHEM-Instrument on AMPTE/CCE, in *Solar Wind-Magnetosphere Coupling*, edited by Y. Kamide and J. A. Slavin, pp. 697–705.

Thomsen, M. F., J. E. Borovsky, D. J. McComas, and M. R. Collier (1998), Variability of the ring current source population, *Geophys. Res. Lett.*, *25*(14), 3481–3484.

Wilson, G. R., D. M. Ober, G. A. Germany, and E. J. Lund (2004), Nightside auroral zone and polar cap ion outflow as a function of substorm size and phase, *J. Geophys. Res.*, *109*, A02206, doi:10.1029/2003JA009835.

Yan, G. Q., C. Shen, Z. X. Liu, C. M. Carr, H. Rème, and T. L. Zhang (2005), A statistical study on the correlations between plasma sheet and solar wind based on DSP explorations, *Ann. Geophys.*, *23*, 2961–2966.

Yau, A. W., and M. André (1997), Sources of ion outflow in the high latitude ionosphere, *Space Sci. Rev.*, *80*, 1–25.

Yau, A. W., W. K. Peterson, and E. G. Shelley (1988), Quantitative parametrization of energetic ionospheric ion outflow, in *Modeling Magnetospheric Plasma, Geophys. Monogr. Ser.*, vol. 44, edited by T. E. Moore and J. H. Waite Jr., pp. 211–217, AGU, Washington, D. C.

Young, D. T., H. Balsiger, and J. Geiss (1982), Correlations of magnetospheric ion composition with geomagnetic and solar activity, *J. Geophys. Res.*, *87*(A11), 9077–9096.

C. W. Carlson and J. P. McFadden, Space Sciences Laboratory, University of California, Berkeley, CA 94720, USA. (cwc@ssl.berkeley.edu; mcfadden@ssl.berkeley.edu)

E. J. Lund, Space Science Center, University of New Hampshire, Durham, NH 03824, USA. (eric.lund@unh.edu)

Y. Miyoshi, K. Seki, and Y. Yao, Solar-Terrestrial Environment Laboratory, Nagoya University, Nagoya, Aichi 464-8601, Japan. (miyoshi@stelab.nagoya-u.ac.jp; seki@stelab.nagoya-u.ac.jp; yaoyao@stelab.nagoya-u.ac.jp)